
UniZyme: A Unified Protein Cleavage Site Predictor Enhanced with Enzyme Active-Site Knowledge

Chenao Li¹ Shuo Yan² Enyan Dai²

Abstract

Enzyme-catalyzed protein cleavage is essential for many biological functions. Accurate prediction of cleavage sites can facilitate various applications such as drug development, enzyme design, and a deeper understanding of biological mechanisms. However, most existing models are restricted to an individual enzyme, which neglects shared knowledge of enzymes and fails to generalize to novel enzymes. Thus, we introduce a unified protein cleavage site predictor named UniZyme, which can generalize across diverse enzymes. To enhance the enzyme encoding for the protein cleavage site prediction, UniZyme employs a novel biochemically-informed model architecture along with active-site knowledge of proteolytic enzymes. Extensive experiments demonstrate that UniZyme achieves high accuracy in predicting cleavage sites across a range of proteolytic enzymes, including unseen enzymes. The code is available in <https://anonymous.4open.science/r/UniZyme-4A67>.

1. Introduction

In the enzyme-catalyzed protein hydrolysis, protein will split at cleavage sites under the catalysis of proteolytic enzymes. This process is illustrated in Fig. 1. And it is crucial for a variety of physiological processes, including cell proliferation, immune response, and cell death, etc (Dixit, 2023). The positions of enzyme-catalyzed cleavage sites are determined by multiple factors. Accurate prediction of enzyme-catalyzed cleavage sites in the substrate proteins facilitates the identification of therapeutic targets and guides drug design (Turk, 2006). For instance, abnormal protein hydrolysis is closely associated with cancer, viral infections, and neurodegenerative diseases, and predicting the cleavage

sites of abnormal proteins under pathological conditions can reveal biomarkers or intervention targets. (McCauley & Rudd, 2016; Liu et al., 2021). Additionally, in the design of enzyme inhibitors or prodrugs, identifying key cleavage peptides, such as those cleaved under the catalysis of HIV enzyme, helps enhance drug specificity and minimize off-target effects (Devroe et al., 2005; Lv et al., 2015).

Cleavage sites of proteins with proteolytic enzymes can be identified through peptide specificity assays or high-throughput mass spectrometry, but these experimental methods are often challenging and expensive (Zheng et al., 2020). Therefore, developing efficient computational tools to complement experimental work is highly valuable. Recent studies have employed deep learning and traditional machine learning methods to advance the prediction of protein cleavage sites. For example, CAT3 (Ayyash et al., 2012) predicts caspase-3 cleavage sites based on position-specific scoring matrices (PSSM). ProsperousPlus (Li et al., 2023) integrates multiple methods to comprehensively evaluate cleavage site predictions.

However, existing methods generally focus on an individual enzyme system. In contrast, many real-world scenarios require understanding how proteins are cleaved by different proteolytic enzymes. For instance, predicting off-target effects of protein therapeutics demands identifying potential cleavage sites for every relevant proteolytic enzyme in the human body's complex environment (Werle & Bernkop-Schnürch, 2006). Although one could train separate predictors for each enzyme, this approach neglects crucial information shared among distinct enzyme-substrate interactions. In addition, the enzyme-specific model lacks the ability to deal with unseen enzymes, limiting its ability to predict cleavage sites for less-studied and de novo enzymes (Liu et al.). Therefore, it is crucial to develop a unified protein cleavage site predictor that can generalize across a diverse range of proteolytic enzymes.

To develop a unified protein cleavage site predictor for diverse proteolytic enzymes, the information of enzyme should be extracted and incorporated for the prediction. However, due to substantial cost of biological experiments, existing cleavage site databases only cover a small number of proteolytic enzymes (Tab. 1), which significantly

¹Institute of Biophysics, Bei Jing, China ²Department of AI Trust, Hong Kong University of Science and Technology (Guangzhou), Guangzhou, China. Correspondence to: Enyan Dai <enyandai@hkust-gz.edu.cn>.

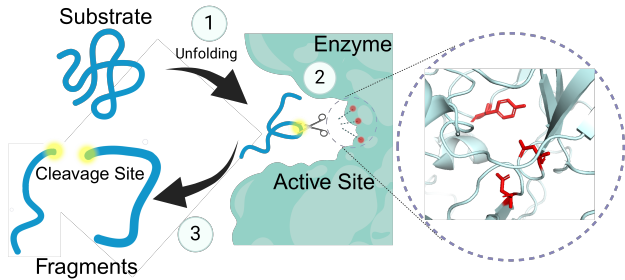


Figure 1. Illustration of the enzyme-catalyzed protein hydrolysis.

challenge the learning of enzyme information encoder. Despite the limited coverage of enzymes in existing cleavage site datasets, many proteolytic enzymes are annotated with their active sites, which is the core functional region for catalyzing the protein hydrolysis. Specifically, the unique physicochemical environment of these active sites enables recognition of target substrates and lowers the activation energy required for cleaving specific peptide bonds. Therefore, we propose to leverage redundant knowledge of enzyme active sites to enhance the modeling of enzymes in enzyme-catalyzed protein cleavage sites.

However, it is non-trivial to achieve a unified cleavage site predictor enhanced with enzyme active-site knowledge. Two major challenges remain to be resolved. *First*, the cleavage process is influenced by various factors of enzymes such as 3D structures and environments of active sites. Check this. Hence, how to design the the architecture of enzyme encoder to effectively capture useful information for enzyme-catalyzed cleavage site prediction? *Second*, the active site regions of enzymes determine the specificity and efficiency of enzymatic hydrolysis. How can we leverage this rich information of enzyme active sites to improve cleavage site prediction? In an attempt to address the challenges, we propose a novel framework named UniZyme. More specifically, a biochemically-informed enzyme encoder is deployed along with the active site-aware pooling to produce high-quality enzyme representations. We further augment the enzyme encoder by pretraining on a supplemented enzyme set for active-site prediction. Furthermore, a joint training of enzyme active site prediction and substrate cleavage site prediction is applied in UniZyme. In summary, our main contributions are:

- We investigate a novel and crucial problem of building a unified protein cleavage site predictor that generalizes across diverse proteolytic enzymes;
- We propose a novel framework UniZyme that effectively integrates the enzyme active-site knowledge to enhance the cleavage site prediction in enzyme-protein interaction;
- Extensive experiments demonstrate the effectiveness of our UniZyme in predicting cleavage sites of substrate proteins for both seen and unseen proteolytic enzymes.

Table 1. Statistics of Cleavage Sites Data in MEROPS.

#Proteolytic Enzyme	#Substrate	Enzyme-Substrate Ratio
866	10146	11.45

2. Problem Formulation

In this section, we firstly introduce the preliminaries of enzyme-catalyzed protein hydrolysis. Then, we present the formal problem definition of protein cleavage site prediction with enzyme active-site knowledge.

2.1. Preliminaries of Protein Hydrolysis

Cleavage Sites in Protein Hydrolysis. *Protein hydrolysis* is a biochemical process where proteins are broken down into smaller fragments such as amino acids and peptides under the catalysis of proteolytic enzymes. As illustrated in Fig. 1, during the protein hydrolysis, proteolytic enzymes will firstly recognize specific amino acid sequences or structural motifs within unfold substrate proteins. Then, the enzymes catalyze the cleavage of peptide bonds at the *cleavage site*, leading to the formation of smaller peptide fragments or individual amino acids. The positions of cleavage sites are governed by various factors including substrate’s amino acid composition, spatial conformation, and unique properties of the enzyme (Klein et al., 2018; Verma et al., 2022; Turk et al., 2001). In therapeutic contexts, precisely designed enzymes can degrade disease-associated proteins while minimizing off-target effects (Tandon et al., 2021; Meghwanshi et al., 2020). Moreover, cleavage site prediction could pinpoint key molecular regions for therapeutic intervention in the development of targeted peptide-based drugs (Radchenko et al., 2019).

Current Framework of Cleavage Site Prediction. Recent studies have employed machine learning models to predict cleavage sites (Wang et al., 2024; Fu et al., 2014; Verspurten et al., 2009; Li et al., 2019; 2020). However, these methods generally train an independent model for each enzyme, which only predict the cleavage sites of substrate proteins under the catalysis of one specific enzyme. Specifically, let \mathcal{P}^s denote the substrate protein, this enzyme-specific cleavage site predictor aims to learn the $f : \mathcal{P}^s \rightarrow \mathbf{c}^{e,s}$, where $\mathbf{c}^{e,s} \in \{0, 1\}^{|\mathcal{P}^s|}$ denotes the labels of cleavage site with the enzyme \mathcal{P}^e . However, the training of enzyme-specific model excludes the valuable interaction knowledge from other enzyme-protein systems. In addition, the enzyme-specific model cannot generalize to unseen enzymes, which significantly limits its application in de novo enzyme design. Therefore, it is crucial to develop a unified cleavage site predictor capable of identifying cleavage sites in substrate proteins across various enzymes.

Data for Cleavage Site Prediction. Tab. 1 presents statistics from the MEROPS cleavage site database. Due to the

high cost of experimental assays, MEROPS (Rawlings et al., 2012) primarily includes 866 commonly used proteolytic enzymes, which collectively target 10,146 protein substrates. This limited enzyme coverage poses a significant challenge for developing a unified cleavage site predictor that generalizes across diverse enzyme–substrate systems.

2.2. Preliminaries of Active Sites in Enzyme

During enzyme-catalyzed protein hydrolysis, the active site provides a specialized environment that lowers the activation energy required for peptide bond cleavage. The illustration of active site of the protein can be found in Fig. 1. With the active sites, enzymes can selectively recognize and bind target substrates, which further enables the cleavage of specific peptide bonds within substrate proteins (Selvaraj et al., 2022). Therefore, the active sites plays a crucial role in substrate cleavage. Hence, incorporating active site information can benefit the modeling of the enzyme-catalyzed protein hydrolysis, thereby enhancing the cleavage site prediction.

Resources for Active Sites. Thanks to the lower cost in annotating active sites of enzymes, UniProt (Consortium, 2024) provides 10,749 high-quality proteolytic enzymes with labeled active sites across multiple organisms. Because most of the entries are synthetic substrates instead of natural proteins, these data cannot be directly utilized for cleavage site prediction. However the rich information of active sites would be helpful in modeling the enzyme to facilitate the cleavage site prediction in protein hydrolysis.

2.3. Problem Definition

In protein hydrolysis, both enzyme \mathcal{P}^e and substrate \mathcal{P}^s are proteins composed of amino acid residues that fold into 3D structures. We denote a protein of length N by $\mathcal{P} = (\mathbf{X}, \mathbf{R})$, where $\mathbf{X} \in \mathbb{R}^{N \times d}$ is the feature matrix of N residues, $\mathbf{R} \in \mathbb{R}^{N \times 3}$ denotes the 3D positions of residues. We denote $\mathbf{c}^{e,s} \in \{0, 1\}^{|\mathcal{P}^s|}$ as the cleavage site label for the substrate protein \mathcal{P}^s under the catalysis of enzyme \mathcal{P}^e . The training data for cleavage site prediction can be represented as $\mathcal{D}_c = \{(\mathcal{P}_i^e, \mathcal{P}_i^s, \mathbf{c}_i^{e,s})\}_{i=1}^{|\mathcal{D}_c|}$. In this work, we propose to enhance the cleavage site prediction with the active site information of enzymes. Hence, we will also utilize a set of enzymes labeled with active sites $\mathbf{a} \in \{0, 1\}^{|\mathcal{P}^e|}$, which is denoted as $\mathcal{D}_a = \{(\mathcal{P}_i^e, \mathbf{a}_i)\}_{i=1}^{|\mathcal{D}_a|}$.

During the test phase, we will predict the cleavage site for each pair of test enzymes and substrates $(\mathcal{P}_t^e, \mathcal{P}_t^s)$. The active sites of test enzymes will not be available for inference. And the test enzyme \mathcal{P}_t^e can be either seen ,i.e, $\mathcal{P}_t^e \in \mathcal{D}_c$ or unseen, i.e, $\mathcal{P}_t^e \notin \mathcal{D}_c$, which correspond to the applications on well-studied enzymes and de novo enzymes, respectively. For each test substrate protein \mathcal{P}_t^s , its cleavage site with the test enzyme \mathcal{P}_t^e is not included in the training set \mathcal{D}_c . With

the above notations and descriptions, the formal definition of building a unified cleavage site predictor can be given by:

Problem 1. *Given the dataset \mathcal{D}_c annotated for cleavage site prediction and the supplemented dataset \mathcal{D}_a containing enzymes active sites, we aim to obtain a unified cleavage site predictor:*

$$f : (\mathcal{P}^e, \mathcal{P}^s) \rightarrow \mathbf{c}^{e,s}, \quad (1)$$

which can accurately predict the cleavage site of test substrate proteins \mathcal{P}_t^e under the catalysis of test proteolytic enzymes \mathcal{P}_t^s . Note that the test enzymes can be either seen or unseen during the training phase.

3. Methodology

In this section, we give the details of the proposed UniZyme. As the Fig. 2 shows, apart from the substrate encoder, UniZyme deploys an enzyme encoder to enable the generalization of cleavage site prediction across various enzymes. In addition, active site information in protein hydrolysis is incorporated into enzyme encoder training to enhance cleavage site prediction. Two main challenges remain to be addressed: (i) how to design the enzyme encoder to preserve critical information for cleavage site prediction? (ii) how to leverage the rich information of enzyme active sites to improve the cleavage site prediction?

To tackle the above challenges, our UniZyme deploys a biochemically-informed enzyme encoder which augments the graph transformer with enzyme energy frustration (Dai et al., 2024). Furthermore, UniZyme employs active site-aware pooling to preserve the enzyme’s information crucial for protein hydrolysis. To facilitate enzyme representation learning, UniZyme first pretrains the enzyme encoder using active site prediction with the supplemented enzyme set. Then, a joint loss of active site prediction and cleavage site prediction is employed to optimize the UniZyme for accurate cleavage site prediction. Next, we introduce each component in detail.

3.1. Biochemically-Informed Enzyme Encoder

Enzymes’ 3D structures, especially the local environments around their active sites, are crucial for catalyzing protein hydrolysis. Although direct active-site annotations are often unavailable for test data, recent studies indicate that local energetic frustration can identify functionally important regions (Freiberger et al., 2019). Building on these insights, we propose a biochemically-informed enzyme encoder that integrates both the spatial positions of residues and their energetic frustration scores (Dai & Wang, 2021).

Input Features and Backbone. Recent success of AlphaFold and ESMFold demonstrates that protein language models can produce powerful representations from protein

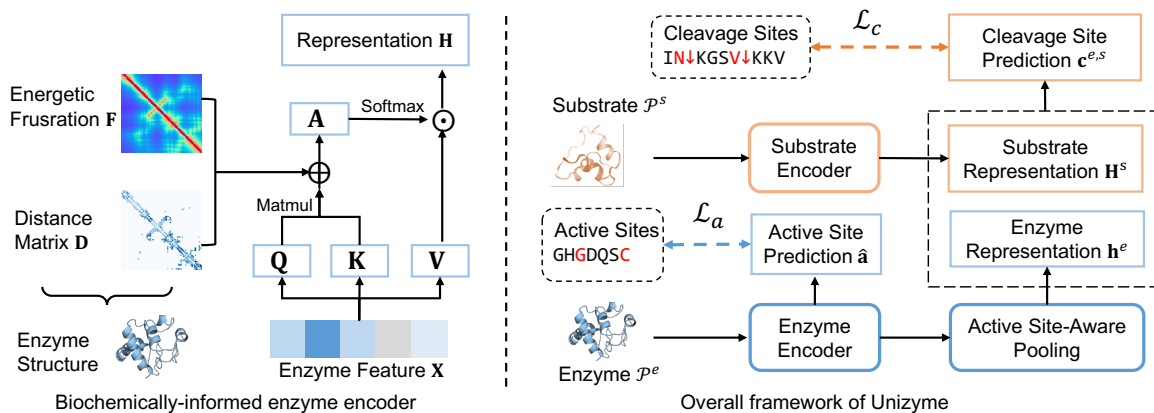


Figure 2. Architecture of biochemically-informed enzyme encoder and overall framework of UniZyme.

sequences for various protein tasks (Lin et al., 2023). Therefore, we initialize the input features of enzymes denoted as \mathbf{X} with their ESM-2 representations. Then, we deploy an extended version of graph transformer (Ying et al., 2021; Jumper et al., 2021) to encode the input features with supplemented biochemical information for cleavage site prediction. Next, we introduce how we extend graph transformer to integrate the energetic frustration and 3D position information.

Encoding Energetic Frustration. Previous studies indicate that local energetic frustration, referring to regions in a protein not optimized for minimal energy, is commonly observed around enzyme active sites and can significantly influence catalysis (Freiberger et al., 2019). To quantify this phenomenon, a frustration score $\mathbf{F}(i, j)$ is computed for each residue pair (i, j) within an enzyme \mathcal{P}^e following (Freiberger et al., 2019):

$$\mathbf{F}(i, j) = \frac{\mathbf{E}(i, j) - \mu_{\text{rand}}(i, j)}{\sigma_{\text{rand}}(i, j)}, \quad (2)$$

where $\mathbf{E}(i, j)$ is the actual interaction energy between residues (i, j) in the enzyme \mathcal{P}^e . $\mu_{\text{rand}}(i, j)$ and $\sigma_{\text{rand}}(i, j)$ represent the mean and standard deviation of interaction energies that derived from randomized configurations (see Appendix C for details). A higher $\mathbf{F}(i, j)$ implies stronger local energetic frustration, suggesting that the residue pair is more likely to belong to a functionally important region. Therefore, we incorporate this frustration score to provide useful biochemical information to the enzyme encoder.

Integrating Energy and 3D Position in Transformer. Following prior works (Luo et al., 2023), we encode the 3D positions by computing pair-wise distance between residues:

$$\mathbf{D}(i, j) = \|\mathbf{r}_i - \mathbf{r}_j\|_2, \quad (3)$$

where $\mathbf{r}_i \in \mathbb{R}^3$ is the $\text{C}\alpha$ -atom coordinate of residue i . Both energetic frustration score and distance matrix capture pair-wise relationships akin to the spatial encoding in graph transformers. Therefore, following Transformer-M (Luo et al.,

2023), we locate those pair-wise signals to provide complementary information for the self-attention score computation. Concretely, for a enzyme $\mathcal{P}^e = (\mathbf{X}, \mathbf{R})$, we process both $\mathbf{F}(i, j)$ and distance matrix $\mathbf{D}(i, j)$ with a Gaussian Basis Kernel function followed by a MLP:

$$\begin{aligned} \Phi_{i,j}^{\text{energy}} &= \text{MLP}(\phi_{\text{energy}}(\mathbf{F}(i, j))) \\ \Phi_{i,j}^{\text{dist}} &= \text{MLP}(\phi_{\text{dist}}(\mathbf{D}(i, j))), \end{aligned} \quad (4)$$

where ϕ_{energy} and ϕ_{dist} denote the learnable Gaussian Basis Kernel function that can map energy frustration score and distance score to a d -dimensional vector (See Appendix C for more details). MLP is further deployed to transform these vectors to the space of attention scores.

We then add the resulting $\Phi_{(i,j)}^{\text{dist}}$ and $\Phi_{(i,j)}^{\text{energy}}$ as bias terms to the self-attention mechanism. Denote $\mathbf{A}_{i,j}^k$ as the (i, j) -element of the Query-Key product matrix in k -th attention layer, we have:

$$\begin{aligned} \mathbf{A}_{i,j}^k &= \frac{(\mathbf{h}_i^{k-1} \mathbf{W}_Q)(\mathbf{h}_j^{k-1} \mathbf{W}_K)^T}{d} + \Phi_{i,j}^{\text{energy}} + \Phi_{i,j}^{\text{dist}} \\ \mathbf{H}^k &= \text{softmax}(\mathbf{A}^k) \mathbf{H}^{k-1} \mathbf{W}_V, \end{aligned} \quad (5)$$

where $\mathbf{H}^k \in \mathbb{R}^{N \times d}$ denotes the updated representation matrix. And \mathbf{W}_Q , \mathbf{W}_K , and \mathbf{W}_V are projection matrices for the query, key, and value transformations. Following Transformer-M (Luo et al., 2023), $\Phi_{i,j}^{\text{energy}}$ and $\Phi_{i,j}^{\text{dist}}$ are shared for all layers.

3.2. Enhancing Enzyme Representation Learning with Active Site Knowledge

To incorporate crucial active-site knowledge into enzyme representation learning, we use three strategies: (i) an auxiliary active-site prediction task to strengthen the enzyme encoder, (ii) large-scale pretraining for active-site prediction to capture general catalytic patterns, and (iii) an active-site-aware pooling mechanism that emphasizes catalysis-related residues. Next, we give more details.

Active Site Prediction. Active sites play a key role in catalyzing the protein cleavage. Hence, active-site information can provide essential understandings of enzyme functions. As a result, we deploy the active site prediction as the auxiliary task to benefit the enzyme encoder training by:

$$\hat{a}_i = \text{sigmoid}(\mathbf{h}_i \cdot \mathbf{w}_a), \quad (6)$$

where $\hat{a}_i \in [0, 1]$ denotes the probability of the i -th residue being the active site, $\mathbf{h}_i \in \mathbb{R}^d$ is the representation of i -th residues in the enzyme, and $\mathbf{w}_a \in \mathbb{R}^d$ denotes the learnable parameters for active site prediction.

Pretraining with the Supplemented Enzyme Set \mathcal{D}_a . The number of enzymes annotated in cleavage site database is limited, which poses a significant challenge for the effective training of enzyme encoders (Dai et al., 2023). However, there exists abundant enzyme data annotated with active sites. Therefore, we select enzyme types highly homologous to the target proteolytic enzymes in biological function to expand the pretraining dataset. Formally, the objective function of pretraining the enzyme encoder on the supplemented enzyme set \mathcal{D}_a can be written as:

$$\min_{\theta_e, \mathbf{w}_a} \mathcal{L}_a(\mathcal{D}_a) = \frac{1}{|\mathcal{D}_a|} \sum_{(\mathcal{P}^e, \mathbf{a}) \in \mathcal{D}_a} l_{\text{BCE}}(\hat{\mathbf{a}}, \mathbf{a}), \quad (7)$$

where θ_e denotes the parameters of enzyme encoder. $\hat{\mathbf{a}} = [\hat{a}_1, \dots, \hat{a}_N]$ denotes the probability vector of active site on the enzyme \mathcal{P}^e . l_{BCE} denotes the element-wise binary cross entropy loss. By pretraining on a large corpus of enzyme sequences, we allow the model to capture broader structural and functional patterns common across enzymes.

Active Site-Aware Pooling. To obtain enzyme representation from a sequence of residue representations, a pooling operation such as mean pooling is required. However, residues that are active sites are more critical for enzymatic activity. Hence, intuitively, these active sites should contribute more in the aggregated enzyme representation (Dai & Wang, 2022). Therefore, we design an active site-aware pooling mechanism, whose pooling weights are based on the predicted active site probabilities. Let $\hat{a}_i \in \mathbb{R}^N$ be the predicted probability that i -th residue is an active site in an N -residue enzyme. The active site-aware pooling can be written as:

$$\mathbf{h}^e = \text{softmax}([w_1, \dots, w_N])\mathbf{H}, \quad w_i = f(\hat{a}_i), \quad (8)$$

where $\mathbf{H} \in \mathbb{R}^{N \times d}$ is representations of residues given by the enzyme encoder. $f(\cdot)$ is a learnable function that will map each \hat{a}_i to the pooling weight w_i . With the active site-aware pooling, we would be able to encourages the model to focus on catalytically relevant segments of the enzyme.

3.3. Cleavage Site Prediction

Substrate Protein Encoding. Similar to the enzyme encoding, we use ESM-2 representations to initialize substrate features. Since there is no functional region in substrates, we omit the energetic frustration encoding for the substrate protein. Only input features \mathbf{X}^s and distance matrix \mathbf{D}^s of the substrate \mathcal{P}^s are integrated in the transformer:

$$\mathbf{H}^s = \text{Transformer}(\mathbf{X}^s, \mathbf{D}^s), \quad (9)$$

where $\mathbf{H}^s \in \mathbb{R}^{|\mathcal{P}^s| \times d}$ is the substrate representation. Further implementation details are provided in Appendix C.

Cleavage Site Prediction. During protein hydrolysis, enzymes generally recognize local residue sequences about 15–30 residues in length. To reflect this biological behavior, we predict whether a subsequence of length l in substrate \mathcal{P}^e will be cleaved by enzyme \mathcal{P}^e . Formally, this process can be written by:

$$\hat{c}_t^{e,s} = \text{MLP}(\text{CONCAT}(\mathbf{H}_{t:t+l}^s, \mathbf{h}^e)) \quad (10)$$

where $\mathbf{H}_{t:t+l}^e$ is a contiguous slice taken directly from the substrate representation matrix \mathbf{H}^s and \mathbf{h}^e is the enzyme representation obtained by Eq.(8). The length of the subsequence is set as 31 (15 residues on each side.). The optimization function of cleavage site prediction can be written as:

$$\mathcal{L}_c(\mathcal{D}_c) = \frac{1}{|\mathcal{D}_c|} \sum_{(\mathcal{P}^e, \mathcal{P}^s, \mathbf{c}^{e,s}) \in \mathcal{D}_c} l_{\text{BCE}}(\mathbf{c}^{e,s}, \hat{\mathbf{c}}^{e,s}) \quad (11)$$

where $\hat{\mathbf{c}}^{e,s} = [\hat{c}_1^{e,s}, \dots, \hat{c}_{|\mathcal{P}^s|}^{e,s}]$ denotes the probability vector of cleavage site within the substrate \mathcal{P}^s given the enzyme \mathcal{P}^e . l_{BCE} is the element-wise binary cross entropy loss.

3.4. Final Objective Function

For each enzyme $\mathcal{P}^e \in \mathcal{D}_c$ in the cleavage site database, their active sites are also included in the \mathcal{D}_a . Consequently, we combine the cleavage site prediction loss and the active site prediction to jointly train the whole framework by:

$$\min_{\theta} \mathcal{L}_c(\mathcal{D}_c) + \lambda \mathcal{L}_a(\mathcal{D}_a^c), \quad (12)$$

where θ denotes all parameters in UniZyme including the enzyme encoder, substrate encoder, active prediction module and cleavage site prediction module. $\mathcal{D}_a^c \subset \mathcal{D}_a$ provides the active-site annotations for the enzymes in \mathcal{D}_c .

4. Experiments

In this section, we conduct experiments to answer the following research questions:

- **RQ1:** How does the performance of UniZyme compared to existing models in supervised cleavage site prediction?

Table 2. Comparison of protein cleavage site prediction in a supervised setting. All values are mean \pm std (%). Note that ScreenCap3 and CAT3 are specialized models for the C14.003 enzyme family, which are not applicable to C14.005 and M10.003.

Enzymes	Metric	ScreenCap3	CAT3	ProsperousPlus	Procleave	ReactZyme	ClipZyme	UniZyme
C14.003	ROC-AUC	74.6 \pm 10.2	74.9 \pm 10.1	93.7 \pm 0.6	69.4 \pm 0.9	93.3 \pm 0.2	93.5 \pm 0.1	97.3\pm0.1
	PR-AUC	29.2 \pm 16.0	18.5 \pm 6.2	26.6 \pm 2.1	4.4 \pm 3.7	43.8 \pm 0.8	35.3 \pm 0.9	45.9\pm1.2
C14.005	ROC-AUC	NA	NA	86.6 \pm 0.6	73.0 \pm 0.9	92.9 \pm 0.2	92.3 \pm 0.4	96.2\pm0.1
	PR-AUC	NA	NA	15.9 \pm 0.5	3.5 \pm 0.3	47.6 \pm 0.9	43.2 \pm 1.0	52.2\pm0.9
M10.003	ROC-AUC	NA	NA	79.7 \pm 0.8	65.9 \pm 1.1	81.4 \pm 0.3	82.5 \pm 0.3	87.0\pm0.2
	PR-AUC	NA	NA	5.6 \pm 0.5	2.6 \pm 0.1	6.4 \pm 0.3	5.8 \pm 0.2	7.3\pm0.4

- **RQ2:** How well does UniZyme generalize to cleavage site prediction for zero-shot enzymes?
- **RQ3:** How do the design of biochemically-informed enzyme encoder and utilization of active-site knowledge contribute to the performance of UniZyme?

4.1. Experimental Setup

Dataset Collection. The cleavage site dataset \mathcal{D}_c is sourced from the **MEROPS** database, which provides annotations for roughly 10,000 substrate cleavage sites across 876 enzymes. To ensure manageable sequence lengths, we exclude any enzyme or substrate sequences exceeding 1,500 residues (Dai et al., 2021). We then perform a standard dataset expansion procedure commonly used in cleavage site prediction, yielding approximately 220,000 valid enzyme–substrate pairs. The supplemented dataset \mathcal{D}_a is constructed by combining enzyme active-site annotations from in **MEROPS** (Rawlings et al., 2012) and **UniProt** (Consortium, 2024). Specifically, MEROPS provides active-site information for the enzymes already included in \mathcal{D}_c . We further expand the active site data by retrieving hydrolase enzymes from UniProt with the EC number of 3.4.*.*, resulting to around 10K enzymes with active sites in total. The dataset statistics and dataset collection details can be found in Appendix A.

Evaluation. To demonstrate the generalization ability of UniZyme, we evaluate its performance on protein cleavage site prediction for both seen enzymes (supervised) and unseen enzymes (zero-shot).

- **Supervised Setting:** In this scenario, target enzymes are paired with training substrates whose cleavage sites are available. Following (Li et al., 2023; 2019), we use enzyme family M10.003, C14.003, and C14.005 as supervised benchmarks, and we randomly split their enzyme–substrate pairs in an 8:2 ratio for training and test.
- **Zero-shot Setting:** In this setting, the target enzymes have no labeled cleavage sites in the training data. To rigorously examine generalization, we construct three zero-shot benchmarks from the hydrolase families ,i.e., A01.009 and M10.004. We select 20% of enzymes in each family with $\leq 80\%$ sequence similarity to any

training samples with Needleman-Wunsch global alignment (Needleman & Wunsch, 1970).

Baseline Methods. To evaluate the performance of our model, we compare against two specialized models: **CAT3** (Ayyash et al., 2012), which predicts caspase-3 cleavage sites based on position-specific scoring matrices (PSSM), and **ScreenCap3** (Fu et al., 2014), which focuses on caspase-3 cleavage site prediction by filtering high-quality data to improve prediction accuracy. We also compare with several deep-learning methods for cleavage site prediction on a single enzyme. **Procleave** (Li et al., 2020) introduces substrate structural features to account for structural biases in cleavage sites. **ProsperousPlus** (Li et al., 2023) integrates multiple methods to comprehensively evaluate cleavage site predictions. Additionally, we also compare two SOTA enzyme–substrate interaction models, i.e., **ClipZyme** (Mikhael et al., 2024) and **ReactZyme** (Hua et al., 2024), which are originally designed for predicting reactions catalyzed by enzymes. We extend them to the cleavage site prediction task for comparisons. For ClipZyme, we utilize their pretrained EGNN enzyme encoder to the cleavage site prediction framework to demonstrate the superiority using active-site information in enzyme encoding. For ReactZyme, it deploys a ESM-2+MLP architecture for enzyme encoding. We retrain it on our data since its trained weights are unavailable. See Appendix B for more details.

Implementation Details. We utilized the esm2-t12-35M-UR50D model to generate 480-dimensional input features for both enzymes and substrates. These features are then fed into the transformer-based enzyme encoder and protein encoder. The hyperparameter λ is selected based on the validation performance. Each experiment is conducted with 5 runs with different random seeds. To ensure a fair evaluation, hyperparameters of trainable baselines were selected by validation set. More details are in Appendix C.

4.2. Supervised Cleavage Site Prediction

To answer **RQ1**, we compare our UniZyme with various existing methods in supervised cleavage site prediction, where annotations for training substrates are available. The compared methods include two specialized models, i.e.,

ScreenCap3 and CAT3, which are designed exclusively for C14.003. ProsperousPlus and Procleave are recent deep learning methods focusing a single enzyme-substrate system, thus are trained solely with the supervised benchmarks. ReactZyme and ClipZyme are extensions of enzyme-substrate interaction models and utilize the same training data as UniZyme. Notably, ClipZyme employs enzyme encoder weights that were pretrained on the enzyme-substrate reaction task. The results on the supervised benchmarks are given in the Tab. 2, where we observe:

- Methods focusing on a single enzyme generally show poor performance; whereas those trained on multiple enzymes achieve significantly better results. This highlights the advantage of developing a unified cleavage site predictor across diverse proteolytic enzymes.
- Compared with ClipZyme which adopts an enzyme encoder pretrained with the enzyme-substrate reaction task, the proposed UniZyme achieves much better performance. It implies the effectiveness of active-active information in enhancing the enzyme encoder.
- Our UniZyme consistently outperforms the ReactZyme by a large margin. This is because of the deployment of biochemically-informed enzyme encoder and the active-site knowledge.

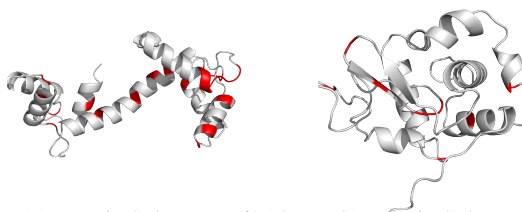
The ROC/PR curves are presented in Appendix D, which shows the similar observations.

Table 3. Cleavage site prediction in zero-shot setting.

Enzyme	Metric (%)	ReactZyme	ClipZyme	UniZyme
M10.004	ROC-AUC	99.20±0.09	98.65±0.15	99.43±0.06
	PR-AUC	71.04±2.80	56.54±3.49	82.82±1.77
A01.009	ROC-AUC	98.59±0.03	98.92±0.03	99.14±0.03
	PR-AUC	18.06±0.31	25.24±0.58	37.51±0.63

4.3. Cleavage Site Prediction for Zero-Shot Enzymes

To answer **RQ2**, we evaluate the performance of UniZyme on the zero-shot benchmarks, where enzymes are unseen during the training phase. Since enzyme-specific models cannot handle new enzymes, we only compare UniZyme to ReactZyme and ClipZyme, both of which can predict cleavage sites for novel enzymes. The results on the zero-shot benchmarks are given in Tab. 3. The ROC/PR curves can be found in Appendix D. From the table, we can observe that our UniZyme consistently outperform the baseline methods. In particular, UniZyme exceeds ReactZyme and ClipZyme by more than 10% in PR-AUC across both enzyme families. This gap is much larger than that of supervised benchmarks. This improvement stems from the utilization of redundant active-site knowledge in the enzyme modeling, promoting the generalization ability of UniZyme to unseen enzymes.



(a) Protein Substrate P62157 (b) Protein Substrate P00698

Figure 3. Visualizations of predicted substrate cleavage sites for HIV-1 enzymes. Predicted cleavage sites are in red color.

4.4. Exploring Substrates of HIV-1 Enzymes

To further demonstrate the generalization ability of our model on unseen enzymes, we applied it to identify potential HIV-1 enzyme substrates and predict their cleavage sites. In Fig. 3, the red residues correspond to high-probability cleavage sites. We present the model’s prediction on an unseen HIV-1 enzyme (MER0019850) acting on a substrate (P62157). This demonstrates that our UniZyme can make accurate predictions even for new, previously unseen enzymes. The predicted cleavage sites on this unseen enzyme show a similar pattern to those observed in other HIV-1 enzymes (DAU, 1991; Tomasselli et al., 1991), further supporting the generalizability of our model for enzyme-substrate interaction tasks. Additionally, our model demonstrates the ability to analyze cleavage sites for any substrate protein interacting with HIV-1 enzymes. For example, as a random test case, our model successfully predicts the cleavage sites of a substrate protein (Uniprot: P00698). This result highlights the model’s capability to explore potential interactions between HIV-1 enzymes and various substrate proteins, providing valuable insights for therapeutic intervention and the development of inhibitors targeting HIV-1 enzymes.

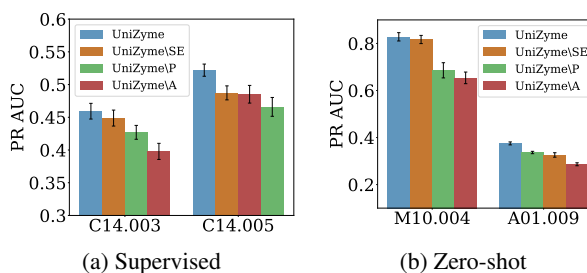


Figure 4. Ablation studies on supervised and zero-shot settings.

4.5. Ablation Studies

To answer **RQ3**, we conduct an ablation study to understand the contributions of biochemically-informed enzyme encoder and the active-site knowledge. To demonstrate the effectiveness of the biochemically-informed enzyme encoder, we remove energy frustration and 3D structure, resulting in a variant named **UniZyme\SE**. To show the benefits brought by pretraining on general enzymes with

active site prediction, we trained a variant, **UniZyme**P, which excludes the enzyme pretraining phase. To further demonstrate the enhancement of active-site knowledge to the model, we remove the active site prediction in the pre-training/training phase. Additionally, the active site-aware pooling is replaced with average pooling, resulting in a variant named **UniZyme**A. Fig. 4 show the PR-AUC scores across different enzyme families in both zero-shot and supervised settings. More details can be found in the Tab. 7 From these results, we observe:

- UniZyme consistently achieves better results than UniZyme\SE, which indicates that structural-energy features in the biochemically-informed enzyme encoder enable stronger generalization and performance.
- UniZyme\
P performs worse than UniZyme, especially on smaller datasets like M10.003. This verifies that pre-training on a supplemented enzyme set produces a more transferable enzyme encoder for cleavage site prediction.
- UniZyme outperforms UniZyme\
A by a large margin. This demonstrates that the active-site knowledge can enhance the enzyme-catalyzed cleavage site prediction.

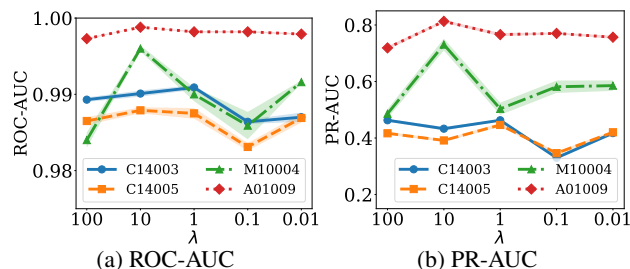


Figure 5. Hyperparameter sensitivity analysis.

4.6. Hyperparameter Analysis

In this subsection, we investigate how the hyperparameter λ affects the UniZyme. λ controls to contribution of active site prediction loss to the training of UniZyme. To explore the hyperparameter analysis, we vary λ as $\{100, 10, 1, 0.1, 0.01\}$ in the training phase of UniZyme. Due to the expensive computational cost in training on the full dataset \mathcal{D}_c , we conduct the hyperparameter analysis with 3% of training data in various enzyme families. Performance on these enzymes are given in Fig. 5. We can find that while $\lambda = 100$ produces competitive ROC-AUC results, it leads to suboptimal PR-AUC. Small values like 0.1 and 0.01 cause a noticeable drop in ROC AUC (e.g. M10.003). Among the tested values, $\lambda = 10$ demonstrates the most consistent performance, achieving strong PR-AUC (e.g., M10.004) while maintaining competitive ROC AUC across datasets such as C14.003 and A01.009. Thus, we selected $\lambda = 10$ as the optimal choice for final training.

5. Related Works

Protein Representation Learning. Protein representation learning aims to effectively capture and represent the structural and functional features of proteins for downstream tasks. Inspired by large language models, recent years have seen the emergence of sequence-based pre-trained models such as ESM (Brandes et al., 2022), and ProtTrans (Elnaggar et al., 2021). In terms of methods that utilize structural information, geometric graph neural networks (Jing et al., 2020; Satorras et al., 2021; Zhang et al., 2022) and transformers with structural constraints (Ying et al., 2021; Luo et al., 2023) have become the widely-used architectures. The pretraining on structural information also facilitate the performance on downstream tasks. Accurate prediction of enzyme-catalyzed reactions requires better modeling of enzymes. ClipZyme (Mikhael et al., 2024) uses EGNN (Satorras et al., 2021) to represent protein graphs and utilizes ESM-2 embeddings to initialize node representations. ReactZyme (Hua et al., 2024), similar to ClipZyme, additionally employs a structure-based protein language model (Su et al., 2023). Although these methods combine structural and contextual features to represent enzymes, they do not incorporate the enzyme’s energy landscape and active-site knowledge, which are crucial for understanding the enzyme’s function and properties.

Cleavage Site Prediction. The early prediction of enzyme-catalyzed cleavage sites relied on substrate sequence patterns, such as CAT3 (Ayyash et al., 2012) and ScreenCap3 (Fu et al., 2014), etc. Recently, machine learning-based methods such as Procleave (Li et al., 2020) and ProsperousPlus (Li et al., 2023) begin incorporating substrate structural features to capture the preferences of cleavage sites. Deep learning methods subsequently revolutionized the field, with studies like DeepCleave (Li et al., 2019) and DeepDigest (Yang et al., 2021) introducing convolutional neural networks and transfer learning to predict protease-specific substrates and cleavage sites, while DeepNeuropePred (Wang et al., 2024) demonstrated the application of protein language models in neuropeptide cleavage prediction. However, the aforementioned methods are all enzyme-specific models, which are only applicable to an individual target enzyme. The crucial information of enzymes’ active sites are not considered either. Therefore, we propose the unified cleavage site predictor enhanced with active-site knowledge.

6. Conclusion and Future work

In this paper, we study a novel problem of developing a unified protein cleavage site predictor for diverse proteolytic enzymes. Specifically, we design a biochemically-informed enzyme encoder and incorporate redundant enzyme active-site information. Our experimental results demonstrate that

UniZyme outperforms baselines by a large margin across various enzyme-substrate families, particularly excelling in zero-shot scenarios. Ablation studies further demonstrate the effectiveness of each proposed module in UniZyme. There are two directions that need further investigation. First, while this study focuses on proteolytic enzymes, we will extend to other categories of enzymes and substrates, and investigate whether enzyme-catalyzed reactions follow scaling law. Second, if more hydrolysis process data becomes available, incorporating dynamic structural information may improve prediction accuracy.

7. Impact Statement

This paper presents work whose goal is to advance the field of Machine Learning. There are many potential societal consequences of our work, none which we feel must be specifically highlighted here.

References

- Cleavage of phosphorylase kinase and calcium-free calmodulin by hiv-1 protease. *Biochemical and Biophysical Research Communications*, 178(3):892–898, 1991. ISSN 0006-291X. doi: [https://doi.org/10.1016/0006-291X\(91\)90975-D](https://doi.org/10.1016/0006-291X(91)90975-D). URL <https://www.sciencedirect.com/science/article/pii/0006291X9190975D>.
- Ayyash, M., Tamimi, H., and Ashhab, Y. Developing a powerful in silico tool for the discovery of novel caspase-3 substrates: a preliminary screening of the human proteome. *BMC Bioinformatics*, 13(1):14, Jan 2012. ISSN 1471-2105. doi: 10.1186/1471-2105-13-14. URL <https://doi.org/10.1186/1471-2105-13-14>.
- Berman, H. M., Westbrook, J., Feng, Z., Gilliland, G., Bhat, T. N., Weissig, H., Shindyalov, I. N., and Bourne, P. E. The protein data bank. *Nucleic Acids Research*, 28(1):235–242, 01 2000. ISSN 0305-1048. doi: 10.1093/nar/28.1.235. URL <https://doi.org/10.1093/nar/28.1.235>.
- Brandes, N., Ofer, D., Peleg, Y., Rappoport, N., and Linial, M. Proteinbert: a universal deep-learning model of protein sequence and function. *Bioinformatics*, 38(8):2102–2110, 2022.
- Consortium, T. U. Uniprot: the universal protein knowledgebase in 2025. *Nucleic Acids Research*, 53(D1):D609–D617, 11 2024. ISSN 0305-1048. doi: 10.1093/nar/gkae1010. URL <https://doi.org/10.1093/nar/gkae1010>.
- Dai, E. and Wang, S. Towards self-explainable graph neural network, 2021. URL <https://arxiv.org/abs/2108.12055>.
- Dai, E. and Wang, S. Towards prototype-based self-explainable graph neural network, 2022. URL <https://arxiv.org/abs/2210.01974>.
- Dai, E., Shu, K., Sun, Y., and Wang, S. Labeled data generation with inexact supervision, 2021. URL <https://arxiv.org/abs/2106.04716>.
- Dai, E., Cui, L., Wang, Z., Tang, X., Wang, Y., Cheng, M., Yin, B., and Wang, S. A unified framework of graph information bottleneck for robustness and membership privacy, 2023. URL <https://arxiv.org/abs/2306.08604>.
- Dai, E., Zhao, T., Zhu, H., Xu, J., Guo, Z., Liu, H., Tang, J., and Wang, S. A comprehensive survey on trustworthy graph neural networks: Privacy, robustness, fairness, and explainability. *Machine Intelligence Research*, 21(6):1011–1061, September 2024. ISSN 2731-5398. doi: 10.1007/s11633-024-1510-8. URL <http://dx.doi.org/10.1007/s11633-024-1510-8>.
- David, A., Islam, S., Tankhilevich, E., and Sternberg, M. J. E. The alphafold database of protein structures: A biologist’s guide. *Journal of Molecular Biology*, 434(2):167336, 2022. doi: 10.1016/j.jmb.2021.167336. URL <https://doi.org/10.1016/j.jmb.2021.167336>. Epub 2021 Oct 29.
- Davtyan, A., Schafer, N. P., Zheng, W., Clementi, C., Wolynes, P. G., and Papoian, G. A. Awsem-md: Protein structure prediction using coarse-grained physical potentials and bioinformatically based local structure biasing. *The Journal of Physical Chemistry B*, 116(29):8494–8503, 07 2012. ISSN 1520-6106. doi: 10.1021/jp212541y. URL <https://doi.org/10.1021/jp212541y>.
- Devroe, E., Silver, P. A., and Engelman, A. Hiv-1 incorporates and proteolytically processes human ndr1 and ndr2 serine-threonine kinases. *Virology*, 331(1):181–189, 2005.
- Dixit, V. M. The road to death: Caspases, cleavage, and pores. *Science Advances*, 9(17):ead2011, 2023.
- Elnaggar, A., Heinzinger, M., Dallago, C., Rehawi, G., Wang, Y., Jones, L., Gibbs, T., Feher, T., Angerer, C., Steinegger, M., et al. Prottrans: Toward understanding the language of life through self-supervised learning. *IEEE transactions on pattern analysis and machine intelligence*, 44(10):7112–7127, 2021.

- Freiberger, M. I., Guzovsky, A. B., Wolynes, P. G., Parra, R. G., and Ferreiro, D. U. Local frustration around enzyme active sites. *Proceedings of the National Academy of Sciences of the United States of America*, 116(10):4037–4043, 2019. doi: 10.1073/pnas.1819859116. URL <https://doi.org/10.1073/pnas.1819859116>.
- Fu, S.-C., Imai, K., Sawasaki, T., and Tomii, K. Screenshot3: Improving prediction of caspase-3 cleavage sites using experimentally verified noncleavage sites. *PROTEOMICS*, 14(17-18):2042–2046, 2014. doi: <https://doi.org/10.1002/pmic.201400002>. URL <https://analyticalsciencejournals.onlinelibrary.wiley.com/doi/abs/10.1002/pmic.201400002>.
- Hua, C., Zhong, B., Luan, S., Hong, L., Wolf, G., Precup, D., and Zheng, S. Reactzyme: A benchmark for enzyme-reaction prediction, 2024. URL <https://arxiv.org/abs/2408.13659>.
- Jing, B., Eismann, S., Suriana, P., Townshend, R. J., and Dror, R. Learning from protein structure with geometric vector perceptrons. *arXiv preprint arXiv:2009.01411*, 2020.
- Jumper, J., Evans, R., Pritzel, A., Green, T., Figurnov, M., Ronneberger, O., Tunyasuvunakool, K., Bates, R., Židek, A., Potapenko, A., et al. Highly accurate protein structure prediction with alphafold. *nature*, 596(7873):583–589, 2021.
- Klein, T., Eckhard, U., Dufour, A., Solis, N., and Overall, C. M. Proteolytic cleavage-mechanisms, function, and "omic" approaches for a near-ubiquitous posttranslational modification. *Chemical Reviews*, 118(3):1137–1168, 2018. doi: 10.1021/acs.chemrev.7b00120. Available from PMC6716334.
- Li, F., Chen, J., Leier, A., Marquez-Lago, T., Liu, Q., Wang, Y., Revote, J., Smith, A. I., Akutsu, T., Webb, G. I., Kurgan, L., and Song, J. Deepcleave: a deep learning predictor for caspase and matrix metalloprotease substrates and cleavage sites. *Bioinformatics*, 36(4):1057–1065, 09 2019. ISSN 1367-4803. doi: 10.1093/bioinformatics/btz721. URL <https://doi.org/10.1093/bioinformatics/btz721>.
- Li, F., Leier, A., Liu, Q., Wang, Y., Xiang, D., Akutsu, T., Webb, G. I., Smith, A. I., Marquez-Lago, T., Li, J., and Song, J. Procleave: Predicting protease-specific substrate cleavage sites by combining sequence and structural information. *Genomics, Proteomics & Bioinformatics*, 18(1):52–64, 05 2020.
- Li, F., Guo, X., Wang, C., Akutsu, T., Webb, G., Coin, L., Kurgan, L., and Song, J. Prosperousplus: a one-stop and comprehensive platform for accurate protease-specific substrate cleavage prediction and machine-learning model construction. *Briefings in Bioinformatics*, 24, 09 2023. doi: 10.1093/bib/bbad372.
- Lin, Z., Akin, H., Rao, R., Hie, B., Zhu, Z., Lu, W., Smetanin, N., Verkuil, R., Kabeli, O., Shmueli, Y., et al. Evolutionary-scale prediction of atomic-level protein structure with a language model. *Science*, 379(6637):1123–1130, 2023.
- Liu, C., Wu, J., Chen, Y., Liu, Y., Zheng, Y., Liu, L., and Zhao, J. Advances in zero-shot prediction-guided enzyme engineering using machine learning. *ChemCatChem*, n/a(n/a):e202401542. doi: <https://doi.org/10.1002/cctc.202401542>. URL <https://chemistry-europe.onlinelibrary.wiley.com/doi/abs/10.1002/cctc.202401542>.
- Liu, F., Chen, R., Song, W., Li, L., Lei, C., and Nie, Z. Modular combination of proteolysis-responsive transcription and spherical nucleic acids for smartphone-based colorimetric detection of protease biomarkers. *Analytical Chemistry*, 93(7):3517–3525, 2021.
- Luo, S., Chen, T., Xu, Y., Zheng, S., Liu, T.-Y., Wang, L., and He, D. One transformer can understand both 2d & 3d molecular data, 2023. URL <https://arxiv.org/abs/2210.01765>.
- Lv, Z., Chu, Y., and Wang, Y. Hiv protease inhibitors: a review of molecular selectivity and toxicity. *HIV/AIDS-Research and palliative care*, pp. 95–104, 2015.
- McCauley, J. A. and Rudd, M. T. Hepatitis c virus ns3/4a protease inhibitors. *Current opinion in pharmacology*, 30:84–92, 2016.
- Meghwanshi, G. K., Kaur, N., Verma, S., Dabi, N. K., Vashishtha, A., Charan, P. D., Purohit, P., Bhandari, H. S., Bhojak, N., and Kumar, R. Enzymes for pharmaceutical and therapeutic applications. *Biotechnology and Applied Biochemistry*, 67(4):586–601, 2020. doi: 10.1002/bab.1919.
- Mikhael, P. G., Chinn, I., and Barzilay, R. Clipzyme: Reaction-conditioned virtual screening of enzymes, 2024. URL <https://arxiv.org/abs/2402.06748>.
- Needleman, S. B. and Wunsch, C. D. A general method applicable to the search for similarities in the amino acid sequence of two proteins. *Journal of Molecular Biology*, 48(3):443–453, March 1970. ISSN 0022-2836. doi: 10.1016/0022-2836(70)90057-4.

- Parra, R. G., Schafer, N. P., Radusky, L. G., Tsai, M.-Y., Guzovsky, A. B., Wolynes, P. G., and Ferreiro, D. U. Protein frustratometer 2: a tool to localize energetic frustration in protein molecules, now with electrostatics. *Nucleic Acids Research*, 44(W1):W356–360, 2016. doi: 10.1093/nar/gkw304. URL <https://doi.org/10.1093/nar/gkw304>. Epub 2016 Apr 29.
- Radchenko, T., Fontaine, F., Moretoni, L., and Zamora, I. Software-aided workflow for predicting protease-specific cleavage sites using physicochemical properties of the natural and unnatural amino acids in peptide-based drug discovery. *PLOS ONE*, 14(1):e0199270, 2019. doi: 10.1371/journal.pone.0199270. URL <https://doi.org/10.1371/journal.pone.0199270>.
- Rawlings, N. D., Barrett, A. J., and Bateman, A. Merops: the database of proteolytic enzymes, their substrates and inhibitors. *Nucleic Acids Research*, 40(Database issue): D343–D350, 2012. doi: 10.1093/nar/gkr987. URL <http://merops.sanger.ac.uk>. Available from PMC3245014.
- Satorras, V. G., Hoogeboom, E., and Welling, M. E (n) equivariant graph neural networks. In *International conference on machine learning*, pp. 9323–9332. PMLR, 2021.
- Selvaraj, C., Rudhra, O., Alothaim, A. S., Alkhanani, M., and Singh, S. K. Chapter three - structure and chemistry of enzymatic active sites that play a role in the switch and conformation mechanism. In Donev, R. (ed.), *Protein Design and Structure*, volume 130 of *Advances in Protein Chemistry and Structural Biology*, pp. 59–83. Academic Press, 2022. doi: <https://doi.org/10.1016/bs.apcsb.2022.02.002>. URL <https://www.sciencedirect.com/science/article/pii/S1876162322000165>.
- Su, J., Han, C., Zhou, Y., Shan, J., Zhou, X., and Yuan, F. Saprot: Protein language modeling with structure-aware vocabulary. *bioRxiv*, pp. 2023–10, 2023.
- Tandon, S., Sharma, A., Singh, S., Sharma, S., and Sarma, S. J. Therapeutic enzymes: Discoveries, production and applications. *Journal of Drug Delivery Science and Technology*, 63:102455, 2021. ISSN 1773-2247. doi: <https://doi.org/10.1016/j.jddst.2021.102455>. URL <https://www.sciencedirect.com/science/article/pii/S1773224721001350>.
- Tomasselli, A. G., Howe, W. J., Hui, J. O., Sawyer, T. K., Reardon, I. M., DeCamp, D. L., Craik, C. S., and Henrikson, R. L. Calcium-free calmodulin is a substrate of proteases from human immunodeficiency viruses 1 and 2. *Proteins: Structure, Function, and Bioinformatics*, 10(1): 1–9, 1991. doi: <https://doi.org/10.1002/prot.340100102>. URL <https://onlinelibrary.wiley.com/doi/abs/10.1002/prot.340100102>.
- Turk, B. Targeting proteases: successes, failures and future prospects. *Nature reviews Drug discovery*, 5(9):785–799, 2006.
- Turk, B. E., Huang, L. L., Piro, E. T., and Cantley, L. C. Determination of protease cleavage site motifs using mixture-based oriented peptide libraries. *Nature Biotechnology*, 19(7):661–667, 2001. ISSN 1546-1696. doi: 10.1038/90273. URL <https://doi.org/10.1038/90273>.
- Verma, A., Åberg Zingmark, E., Sparrman, T., Mush-taq, A. U., Rogne, P., Grundström, C., Bertsson, R., Sauer, U. H., Backman, L., Nam, K., Sauer-Eriksson, E., and Wolf-Watz, M. Insights into the evolution of enzymatic specificity and catalysis: From asgard archaea to human adenylate kinases. *Science Advances*, 8(44):eabm4089, 2022. doi: 10.1126/sciadv.abm4089. URL <https://www.science.org/doi/abs/10.1126/sciadv.abm4089>.
- Verspurten, J., Gevaert, K., Declercq, W., and Vandenebeele, P. Sitepredicting the cleavage of proteinase substrates. *Trends in Biochemical Sciences*, 34(7):319–323, 2009. ISSN 0968-0004. doi: <https://doi.org/10.1016/j.tibs.2009.04.001>. URL <https://www.sciencedirect.com/science/article/pii/S0968000409001017>.
- Wang, L., Zeng, Z., Xue, Z., and Wang, Y. Deep-neuropepred: A robust and universal tool to predict cleavage sites from neuropeptide precursors by protein language model. *Computational and Structural Biotechnology Journal*, 23:309–315, 2024. ISSN 2001-0370. doi: <https://doi.org/10.1016/j.csbj.2023.12.004>. URL <https://www.sciencedirect.com/science/article/pii/S2001037023004786>.
- Werle, M. and Bernkop-Schnürch, A. Strategies to improve plasma half life time of peptide and protein drugs. *Amino Acids*, 30(4):351–367, 2006. doi: 10.1007/s00726-005-0289-3. URL <https://doi.org/10.1007/s00726-005-0289-3>.
- Wu, R., Ding, F., Wang, R., Shen, R., Zhang, X., Luo, S., Su, C., Wu, Z., Xie, Q., Berger, B., Ma, J., and Peng, J. High-resolution de novo structure prediction from primary sequence. *bioRxiv*, 2022. doi: 10.1101/2022.07.21.500999. URL <https://www.biorxiv.org/content/early/2022/07/22/2022.07.21.500999>.
- Yang, J., Gao, Z., Ren, X., Sheng, J., Xu, P., Chang, C., and Fu, Y. Deepdigest: prediction of protein proteolytic digestion with deep learning. *Analytical Chemistry*, 93(15):6094–6103, 2021.

Ying, C., Cai, T., Luo, S., Zheng, S., Ke, G., He, D., Shen, Y., and Liu, T.-Y. Do transformers really perform badly for graph representation? *Advances in neural information processing systems*, 34:28877–28888, 2021.

Zhang, Z., Xu, M., Jamasb, A., Chenthamarakshan, V., Lozano, A., Das, P., and Tang, J. Protein representation learning by geometric structure pretraining. *arXiv preprint arXiv:2203.06125*, 2022.

Zheng, J., Strutzenberg, T. S., Reich, A., Dharmarajan, V., Pascal, B. D., Crynen, G. C., Novick, S. J., Garcia-Ordóñez, R. D., and Griffin, P. R. Comparative analysis of cleavage specificities of immobilized porcine pepsin and nepenthesin ii under hydrogen/deuterium exchange conditions. *Analytical Chemistry*, 92(16): 11018–11028, 08 2020. ISSN 0003-2700. doi: 10.1021/acs.analchem.9b05694. URL <https://doi.org/10.1021/acs.analchem.9b05694>. doi: 10.1021/acs.analchem.9b05694.

Table 4. Dataset statistics of training datasets.

Utilization	Datasets	# Substrate-Enzyme Pairs	Enzymes	Substrates
Active site dataset	UniPort	NA	11,530	NA
Cleavage site dataset	MEROPS	197,613	677	7,475

Table 5. Dataset statistics of evaluation benchmarks.

Settings	Datasets	# Substrate-Enzyme Pairs
Supervised	C14.005	1,638
	C14.003	1,462
	M10.003	1,209
Zero-shot	M10.004	204
	A01.009	1,500

A. Details of Data Curation and Benchmark Construction

A.1. Data Curation and Preprocess

For the cleavage dataset, we downloaded enzyme-substrate pairs from the MEROPS (Rawlings et al., 2012) database, collected substrate sequences from the UniProt database, and retrieved enzyme sequences recorded in MEROPS. Additionally, we compared the enzyme sequences between MEROPS and UniProt, excluding those with discrepancies, as such inconsistencies often result from asynchronous updates. To maintain controllable sequence lengths, we filtered out all enzyme and substrate sequences exceeding 1,500 residues.

As for the supplemented enzyme set with active sets, we first searched in the UniProt (Consortium, 2024) database for enzymes with EC numbers starting with 3.4.*.* and filtered for reviewed data. Then, we selected entries with annotated active sites as our pretraining dataset. In addition, proteolytic enzymes in MEROPS are all annotated with active sites, and are combined as the supplemented enzyme set.

Protein structures were collected from the PDB (Berman et al., 2000) and AlphaFoldDB (David et al., 2022). For proteins without available structures in these databases, we generated their structures using OmegaFold (Wu et al., 2022).

A.2. Data Expansion

The MEROPS database classifies enzymes into categories based on their substrate cleavage sites. Enzymes belonging to the same MEROPS category typically share highly similar cleavage-site characteristics (Rawlings et al., 2012). Drawing on previous work, we assume that minor sequence differences among enzymes of the same category can be disregarded. Consequently, the hydrolysis information from a substrate-enzyme pair is extended to all enzymes in that category.

Therefore, we expanded our dataset by matching each substrate not only with the originally mapped enzyme but also with other enzymes in the same MEROPS category. Through this procedure, we obtained approximately 220,000 valid enzyme-substrate pairings, involving 680 unique enzymes.

A.3. Construction of Supervised and Zero-shot Benchmarks

Supervised Setting. We selected three MEROPS categories as supervised benchmarks (M10.003, C14.003, and C14.005), randomly splitting all enzyme-substrate pairs in each category into training and test sets with an 8:2 ratio. To ensure the test substrates were sufficiently distinct from those in training, we first collected all associated substrates for each enzyme category, then computed pairwise sequence similarity using the Needleman-Wunsch algorithm (BLOSUM62, gap opening penalty of 10, gap extension penalty of 0.5). Substrates exhibiting less than 50% similarity to other substrates were considered relatively independent, and we sampled 20% number of all substrates in these independent substrates to form the final test set. This procedure helps to evaluate model generalization to more divergent substrates within the same MEROPS category.

Zero-shot Setting. We constructed a zero-shot benchmark using two other MEROPS categories (A01.009 and M10.004) by

collecting all enzymes in each category and computing their pairwise similarities with the Needleman–Wunsch algorithm (BLOSUM62, gap opening penalty of 10, gap extension penalty of 0.5). We increased the NW threshold to 80% to account for the higher intrinsic similarity of enzymes within each category; enzymes that fell below this threshold were considered distinct and approximately 20% of them were selected to form the zero-shot test set. This ensures no overlap between the zero-shot test enzymes and those used in training.

A.4. Dataset Statistics

In total, the final dataset contains about 200,000 enzyme–substrate pairs. These pairs span multiple MEROPS categories. Detailed distributions of enzyme and substrate pairs are provided in Table 5.

B. Details of Baselines

Below, we provide additional details on how we adapt, retrain, or utilize each baseline for comparison. Unless otherwise specified, all default hyperparameters are used as in the original implementations of these methods. For any required data, we convert our data format accordingly.

Procleave (Li et al., 2020) and **ProsperousPlus** (Li et al., 2023) both provide publicly available code, enabling us to retrain their models within our supervised setting. We use the same training and test sets as those used for our method, specifically for the supervised benchmark. We adopt the default training code from each repository while ensuring that all other settings remain consistent.

ScreenCap3 (Fu et al., 2014) and **CAT3** (Ayyash et al., 2012), specialized for the C14.003 enzyme, do not provide publicly available datasets or source code for retraining. Instead, they each offer a prediction platform: a web server for ScreenCap3 and standalone software for CAT3. We use these platforms to generate predictions on our test set. Since their training data are not publicly accessible, we can only report their performance as is, with the caveat that neither model can be applied to other enzymes.

We also compare with two recent enzyme–substrate interaction models, **ClipZyme** (Mikhael et al., 2024) and **ReactZyme** (Hua et al., 2024), which were originally proposed for reaction rather than cleavage prediction. **ReactZyme** encodes enzymes with an ESM-2 plus MLP pipeline, but since its trained weights are unavailable, we retrain it from scratch on our dataset. **ClipZyme** employs an E(n) Equivariant Graph Neural Network (EGNN) to incorporate structural information into its enzyme encoder. Both models use average-pooling to aggregate the extracted enzyme features and are trained without activation-site loss. To highlight the effect of leveraging active-site knowledge, we keep the original pretrained EGNN for ClipZyme as is and integrate it into our cleavage-site prediction framework, adding only a linear projection layer to interface with the cleavage-site prediction module.

C. Implementation Details

Framework and Hardware. We implemented our models in PyTorch and trained using the Adam optimizer with a learning rate of 1×10^{-4} and a batch size of 48. All experiments were conducted on eight NVIDIA A100 GPUs. We adopted an early stopping strategy with a patience of 3 epochs, monitoring the validation loss to prevent overfitting.

Substrate Representations. Similar to the enzyme pipeline, but without energetic frustration, each residue is embedded by ESM-2 padded to 1500 length. We compute pairwise C α -distances $\mathbf{D}^s(i, j) = \|\mathbf{r}_i - \mathbf{r}_j\|_2$, then applying a reciprocal transform. Each distance entry is processed by a Gaussian basis kernel and MLP, yielding a bias term $\Phi_{i,j}^{\text{dist}}$ added to the attention score:

$$\mathbf{A}_{i,j}^k = \frac{(\mathbf{h}_i^{k-1} \mathbf{W}_Q)(\mathbf{h}_j^{k-1} \mathbf{W}_K)^T}{d} + \Phi_{i,j}^{\text{dist}}, \quad (13)$$

thus incorporating structural information. The substrate representation $\mathbf{H}^s \in \mathbb{R}^{|\mathcal{P}^s| \times d}$ is obtained via

$$\mathbf{H}^s = \text{Transformer}(\mathbf{X}^s, \mathbf{D}^s), \quad (14)$$

with the same architecture as the enzyme encoder but omitting energy-related parameters.

Energy Frustration Calculation. We computed residue-pair frustration using the **Frustratometer** tool (Parra et al., 2016) with AWSEM (Associative Water-mediated Structure and Energy Model) potentials (Davtyan et al., 2012), disabling

electrostatic interactions ($k_{\text{electrostatics}} = 0$) and enforcing a minimum sequence separation of 12 residues between residue pairs. Specifically, for each pair of residues (i, j) in enzyme \mathcal{P}^e , the actual interaction energy $\mathbf{E}(i, j)$ was extracted from the AWSEM potential. To capture local energetic fluctuations, we generated an ensemble of randomized configurations (where the sequence or side-chain identities are shuffled while preserving the protein backbone), thereby obtaining a distribution of interaction energies for each pair.

Let $\mu_{\text{rand}}(i, j)$ and $\sigma_{\text{rand}}(i, j)$ be the mean and standard deviation of these interaction energies over the randomized ensemble. The frustration score $\mathbf{F}(i, j)$ is then computed as:

$$\mathbf{F}(i, j) = \frac{\mathbf{E}(i, j) - \mu_{\text{rand}}(i, j)}{\sigma_{\text{rand}}(i, j)}. \quad (15)$$

A higher $\mathbf{F}(i, j)$ indicates that the local region around residues (i, j) is more frustrated (i.e., further from minimal AWSEM-derived energy). Such regions often correspond to sites of functional importance in enzymes.

To estimate how $\mathbf{E}(i, j)$ deviates from an energetically minimal arrangement, we generated an ensemble of randomized “decoy” configurations for the same residue pair. These decoys preserve global geometry (e.g. backbone coordinates) but shuffle aspects such as side-chain packing or local environment, depending on the chosen protocol within the **Frustratometer**. Each decoy thus provides a distinct pairwise interaction energy. By sampling multiple decoys, we obtain an approximate distribution of energies $\tilde{E}_k(i, j)$, from which we compute:

$$\mu_{\text{rand}}(i, j) = \frac{1}{K} \sum_{k=1}^K \tilde{E}_k(i, j), \quad (16)$$

$$\sigma_{\text{rand}}(i, j) = \sqrt{\frac{1}{K-1} \sum_{k=1}^K \left(\tilde{E}_k(i, j) - \mu_{\text{rand}}(i, j) \right)^2}, \quad (17)$$

where K is the number of randomized decoys (typically on the order of a few hundred in the **Frustratometer**).

Gaussian Basis Kernel Function. Following Transformer-M (Luo et al., 2023), we employ a set of learnable Gaussian basis kernels to transform a scalar input (e.g., the distance $\mathbf{D}(i, j)$ or the frustration score $\mathbf{F}(i, j)$) into a fixed-dimensional embedding. Concretely, suppose we have K Gaussian kernels parameterized by $\{\mu^k, \sigma^k\}_{k=1}^K$. For an input scalar x , the Gaussian basis kernel function $\phi(x)$ is defined as:

$$\phi(x) = \left[\exp\left(-\frac{1}{2}\left(\frac{x-\mu^1}{\sigma^1}\right)^2\right), \exp\left(-\frac{1}{2}\left(\frac{x-\mu^2}{\sigma^2}\right)^2\right), \dots, \exp\left(-\frac{1}{2}\left(\frac{x-\mu^K}{\sigma^K}\right)^2\right) \right]^\top. \quad (18)$$

Each kernel center μ^k and width σ^k is learnable, allowing the model to adaptively capture different regions of the input space. We apply this basis expansion to both $\mathbf{D}(i, j)$ and $\mathbf{F}(i, j)$, producing a K -dimensional vector for each pair (i, j) . An MLP then projects this kernel output into the space of attention biases. We set the number of Gaussian basis functions to $K = 10$, each parameterized by learnable centers μ^k and widths σ^k . Notably, we maintain *separate* sets of Gaussian parameters for the energy and structure channels, ensuring that the model can adaptively learn distinct representations for each.

Training Algorithm. Each sample’s ESM-2 embeddings (padded to length 1500), along with distance and energy frustration matrices, are fed into our model to predict both active-site and cleavage-site residues. We use a weighted binary cross-entropy loss and optimize with Adam for up to 15 epochs, applying early stopping (patience = 3) based on validation loss.

Algorithm 1 Training algorithm of UniZyme**Input:** Supplemented enzyme set \mathcal{D}_a , Cleavage site prediction dataset \mathcal{D}_c , hyperparameters λ **Output:** A unified cleavage site predictor f_θ

- 1: Initialize features of enzyme and substrate protein by ESM-2
- 2: Pretrain enzyme encoder on \mathcal{D}_a with \mathcal{L}_a by Eq.(7)
- 3: **for** epoch = 1 to N **do**
- 4: **for** each batch $(\mathcal{P}^e, \mathcal{P}^s)$ in \mathcal{D}_c **do**
- 5: Compute the distance matrix \mathbf{D}^e , and energetic frustration matrix \mathbf{F}^e from enzyme structure by Eq.(2) and Eq.(3)
- 6: Encode the enzyme by Eq.(5)
- 7: Obtain the enzyme representation with active site-aware pooling by Eq.(8)
- 8: Encode the substrate protein by Eq.(9)
- 9: Predict active sites of enzymes by Eq.(6)
- 10: Predict cleavage sites of substrate proteins by Eq.(10)
- 11: Update θ via $\nabla(\mathcal{L}_c + \lambda\mathcal{L}_a)$
- 12: **end for**
- 13: **if** validation loss increases for 3 epochs **then**
- 14: **break**
- 15: **end if**
- 16: **end for**

D. Additional Experiments and Visualizations

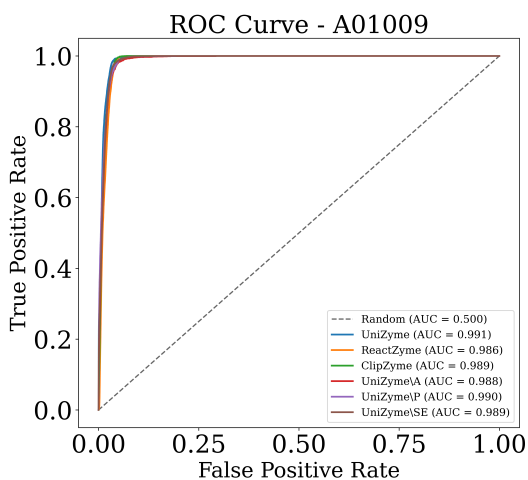
In this section, we present a detailed comparison of the benchmark results across five datasets, including AUC of ROC and PR, as well as the corresponding ROC and PR curves. Additionally, as shown in Fig. 8, we conducted zero-shot testing on all enzymes not included in the training data to evaluate the model’s capability in predicting enzyme active sites.

Table 6. Comparison of model performance on ROC and PR AUC for datasets M10.004 and A01.009.

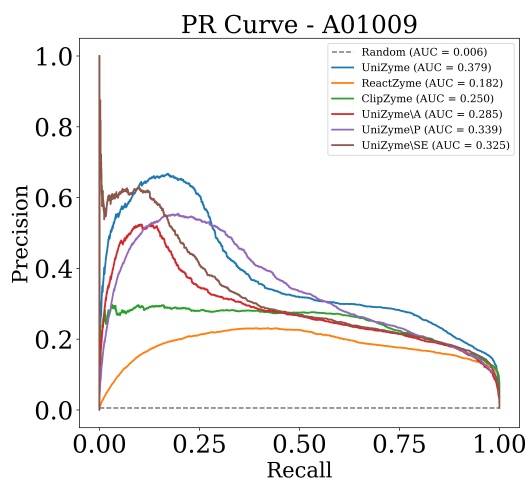
Model	M10.004		A01.009	
	ROC AUC	PR AUC	ROC AUC	PR AUC
UniZyme	0.9943 \pm 0.0006	0.8282 \pm 0.0177	0.9914 \pm 0.0003	0.3751 \pm 0.0063
ReactZyme	0.9920 \pm 0.0009	0.7104 \pm 0.0280	0.9859 \pm 0.0003	0.1806 \pm 0.0031
ClipZyme	0.9865 \pm 0.0015	0.5654 \pm 0.0349	0.9892 \pm 0.0003	0.2524 \pm 0.0058
UniZyme\SE	0.9940 \pm 0.0009	0.8168 \pm 0.0174	0.9892 \pm 0.0004	0.3260 \pm 0.0095
UniZyme\P	0.9876 \pm 0.0015	0.6858 \pm 0.0323	0.9898 \pm 0.0002	0.3364 \pm 0.0050
UniZyme\A	0.9872 \pm 0.0007	0.6537 \pm 0.0247	0.9882 \pm 0.0005	0.2864 \pm 0.0063

Table 7. Ablation study on model performance on ROC and PR AUC for datasets M10.003, C14.005, and C14.003.

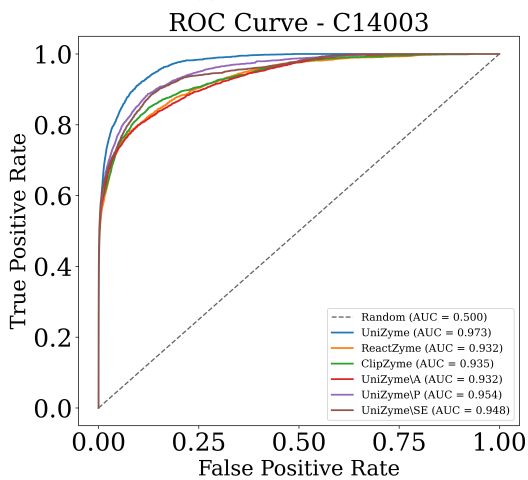
Model	M10.003		C14.005		C14.003	
	ROC AUC	PR AUC	ROC AUC	PR AUC	ROC AUC	PR AUC
UniZyme	0.8702 \pm 0.0020	0.0729 \pm 0.0035	0.9620 \pm 0.0014	0.5220 \pm 0.0093	0.9725 \pm 0.0009	0.4593 \pm 0.0120
UniZyme\SE	0.8210 \pm 0.0030	0.0611 \pm 0.0024	0.9437 \pm 0.0027	0.4873 \pm 0.0107	0.9479 \pm 0.0015	0.4488 \pm 0.0122
UniZyme\P	0.8242 \pm 0.0022	0.0571 \pm 0.0023	0.9367 \pm 0.0040	0.4659 \pm 0.0144	0.9544 \pm 0.0017	0.4270 \pm 0.0106
UniZyme\A	0.8254 \pm 0.0028	0.0608 \pm 0.0023	0.9474 \pm 0.0022	0.4852 \pm 0.0135	0.9316 \pm 0.0018	0.3979 \pm 0.0123



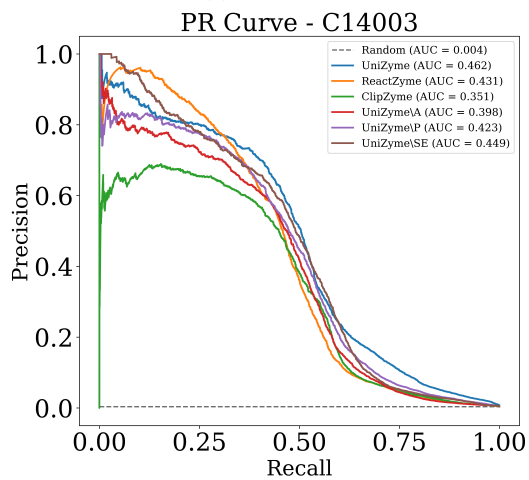
(a) ROC Curve - A01009



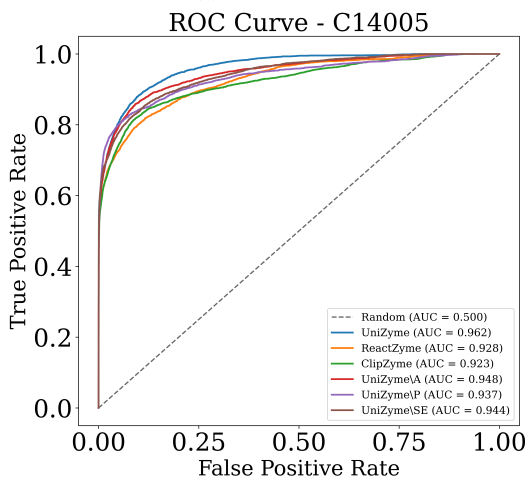
(b) PR Curve - A01009



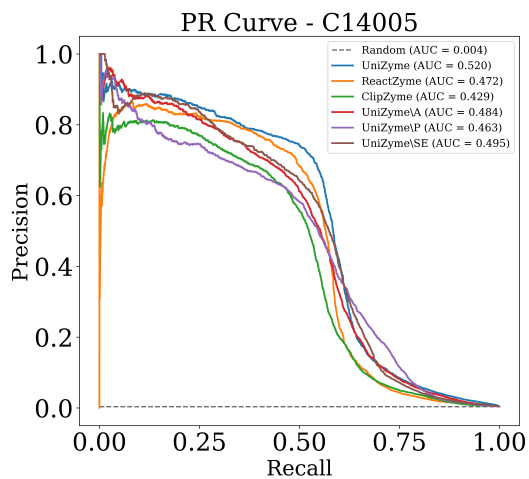
(c) ROC Curve - C14003



(d) PR Curve - C14003



(e) ROC Curve - C14005



(f) PR Curve - C14005

Figure 6. Comparisons in cleavage site prediction under the supervised setting for seen enzymes.

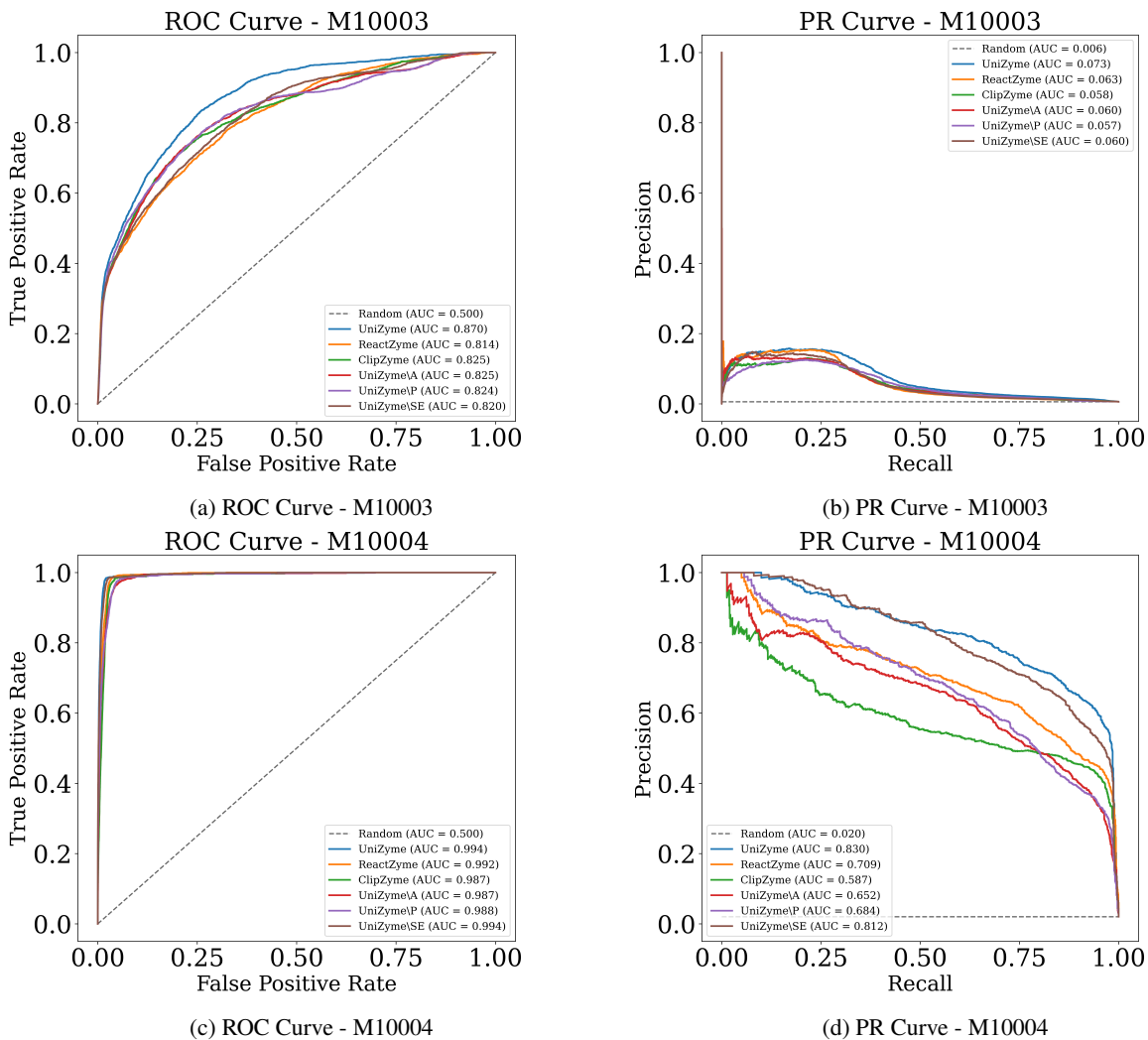


Figure 7. Comparisons in cleavage site prediction under the zero-shot setting for unseen enzymes.

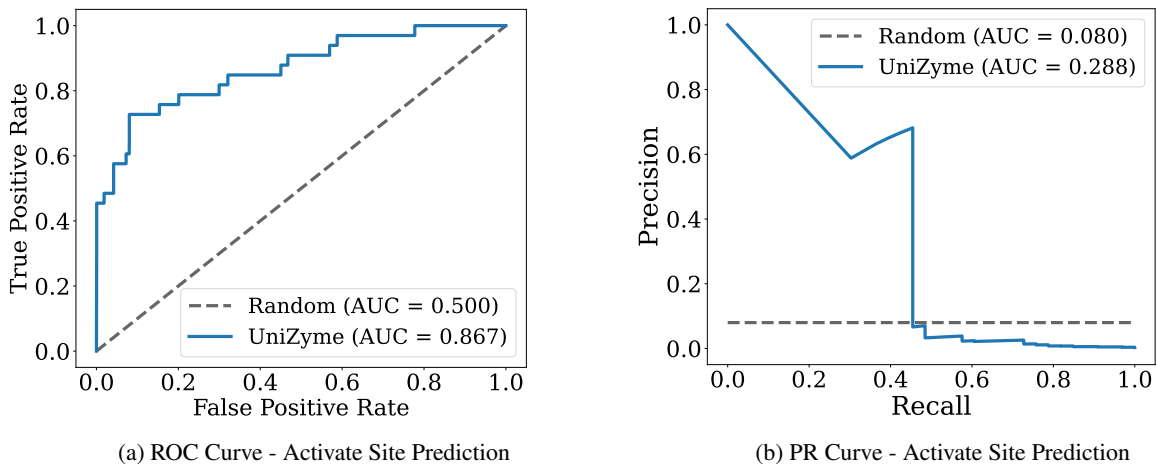


Figure 8. Model performance of activate site prediction